Journal of Magnetic Resonance **144,** 297–304 (2000)
doi:10.1006/jmre.2000.2076, available online at http://www.idealibrary.com on IDEAL®

^{23}Na and ^{1}H NMR Microimaging of Intact Plants

Silvia Olt,* Eva Krötz,† Ewald Komor,† Markus Rokitta,* and Axel Haase*

**Physikalisches Institut Universität Würzburg, 97074 Würzburg, Germany; and †Pflanzenphysiologisches Institut Universität Bayreuth, Bayreuth, Germany*

Received November 1, 1999; revised February 17, 2000

^{23}Na NMR microimaging is described to map, for the first time, the sodium distribution in living plants. As an example, the response of 6-day-old seedlings of *Ricinus communis* to exposure to sodium chloride concentrations from 5 to 300 mM was observed *in vivo* using ^{23}Na as well as ^{1}H NMR microimaging. Experiments were performed at 11.75 T with a double resonant ^{23}Na–^{1}H probehead. The probehead was homebuilt and equipped with a climate chamber. T_1 and T_2 of ^{23}Na were measured in the cross section of the hypocotyl. Within 85 min ^{23}Na images with an in-plane resolution of 156 × 156 μm were acquired. With this spatial information, the different types of tissue in the hypocotyl can be discerned. The measurement time appears to be short compared to the time scale of sodium uptake and accumulation in the plant so that the kinetics of salt stress can be followed. In conclusion, ^{23}Na NMR microimaging promises great potential for physiological studies of the consequences of salt stress on the macroscopic level and thus may become a unique tool for characterizing plants with respect to salt tolerance and salt sensitivity. © 2000 Academic Press

Key Words: **^{23}Na NMR imaging; sodium-23; salt stress; plants; NMR microscopy.**

INTRODUCTION

High salt (NaCl) concentration in soils is highly toxic to most of the higher plants. Cell expansion is hampered as a result of the decreased external water potential. Furthermore buildup of sodium and chloride in the cytoplasm inhibits the metabolic processes. Salinity becomes an increasing problem in irrigated soils and leads to severe limitations in crop yield, especially in arid and semiarid areas.

New salt-tolerant crops are developed by means of breeding new varieties, as well as by genetic engineering. In the literature, salt-tolerant plants are arbitrarily defined as plants standing an external NaCl concentration of more than 100 mM (*1*). A better understanding of salt stress in plants necessitates the investigation of kinetics and mechanisms of sodium uptake, exclusion, and compartmentalization. Until now, information about the sodium pools in plants has been obtained by various highly invasive methods (*1*), such as flame photometry, X-ray microanalysis, ion-selective microelectrodes or ^{22}Na autoradiography. All of these techniques work only with excised tissue or dehydrated or deep frozen samples.

In the past 2 decades, some research has attempted to follow the sodium uptake in plant systems by ^{23}Na NMR spectroscopy, e.g., in cell suspensions (*2–4*) and in excised tissue (*5–8*). Most of these studies were done with the aid of paramagnetic shift reagents (*2–8*). By adding paramagnetic shift reagents (*9*) to the suspending medium, the intra- and extracellular fractions of the sodium signal can be separated. However, shift reagents are of no use on the subcellular level, since they provide no ability to distinguish the cytoplasmatic and the vacuolar pools. In addition, the macromolecular reagents are not taken up by the roots of intact plants. Recently, a general overview of NMR studies of plants (*10*) reviewed the literature on detection of sodium with ^{23}Na NMR spectroscopy.

So far, very little effort has been made to detect macroscopic sodium pools in higher plants by NMR imaging. In the literature, only one example for ^{23}Na NMR imaging of a plant sample can be found (*11*), where a cut piece of a mangrove was investigated.

In the present paper, we demonstrate that high resolution ^{23}Na NMR imaging can map the sodium distribution in intact plants without any perturbation of cell metabolism. This technique ensures localization of the real *in vivo* sites of sodium. It permits repetitive studies on single individual plants. An important advantage over all non-NMR methods is the access to dynamic information and the ease and reliability with which the time course of sodium uptake and localization in plants can be followed. ^{23}Na NMR imaging offers, thus, a unique approach to probe physiological changes in plants as a consequence of increased external salt concentration. For the first time, the stress-induced reaction of the different tissue types in the hypocotyl of an intact growing plant seedling is monitored and the time course of the sodium uptake and its accumulation is observable.

^{23}Na has a natural abundance of 100% and a 9.27% relative NMR sensitivity. Due to its short T_1 relaxation time constant, rapid pulsing and hence fast image acquisition is possible. The chemical shift range of ^{23}Na is negligible. Consequently, signals from each sodium fraction of the tissue are superimposed. The quadrupole character of the nucleus ($I = \frac{3}{2}$) implicates an efficient transverse relaxation mechanism of the outer transitions ($\frac{3}{2} \leftrightarrow \frac{1}{2}$ and $-\frac{3}{2} \leftrightarrow -\frac{1}{2}$) when slowly tumbling macromolecules are present. For that reason the quadrupole interaction causes biexponential T_2 relaxation which may result in partial

1090-7807/00 $35.00

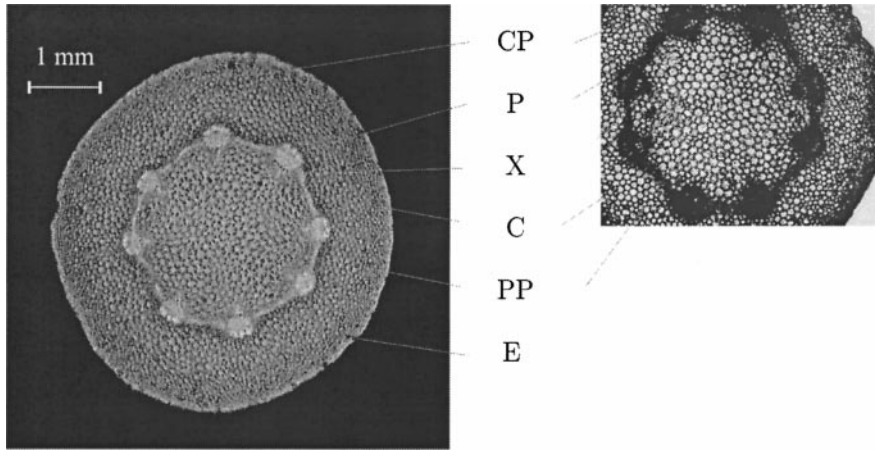

FIG. 1. A cross section of the base of the hypocotyl of a 6-day-old castor bean seedling as seen in a ^{1}H spin-echo image (left) and light microscopy (right). The eight collateral vascular bundles consisting of the triangular xylem (X) and the threefold phloem (P) can be clearly distinguished. They are connected by a ring of meristematic tissue (C) which divides the cortex parenchyma (CP) and the pith parenchyma (PP). Toward the epidermis (E) cell diameter decreases. For the NMR microscopy a spin-echo sequence was chosen to acquire a 512 × 512 data matrix (zero filling to 1024 × 1024) with a FOV of 8 × 8 mm. Slice thickness was 1 mm (TE: 15 ms, TR: 1 s, eight averages).

NMR invisibility of some compartments in biological tissue (*12*). Spatial and temporal resolution are limited by both the low content and the short T_2 values of ^{23}Na in plants.

MATERIALS AND METHODS

The Plant Model

As a plant model system for a nonhalophyte crop, we chose 6-day-old castor bean seedlings (*Ricinus communis* L.), which have been established as a standard model in many NMR investigations (*13–17*). The germinated seedling is about 6 cm high and its cotyledon is still surrounded by the endosperm. With no need for illumination, it can be placed inside the climate chamber probehead without any physiological affects. The arrangement of the eight vascular bundles in a ring facilitates the localization of the different types of tissue, such as xylem, phloem, pith, and cortex parenchyma, as seen in Fig. 1.

Plants were grown hydroponically in darkness individually on top of a glass tube fitting into the probehead. Due to the hydroponic growth, the nutrient solution can be exchanged rapidly and the external salt concentration can be readily calibrated. During germination outside the magnet as well as during the experiments, the plants were aerated from underneath.

Experimental

NMR experiments were performed on a Bruker AMX-500 microscopy system. The magnetic field strength of the 8.9-cm bore magnet is 11.75 T. The actively shielded gradient coils are capable of maximum gradient strengths of 660 mT/m. Minimum rise time is 130 μs. The homebuilt double resonant probehead works with a climate chamber. A detailed description of such a chamber can be found elsewhere (*18*). The glass tube, 15 mm in diameter and 16 cm in length, containing the seedling's roots was built into the probehead and bubbled with air. For calibration purposes, a reference capillary was added as an external standard to a fraction of the plants. Two saddle-shaped coils were placed at the base of the hypocotyl in a concentric crossed manner, the inner one with 8-mm diameter for ^{23}Na imaging and the outer one with 13-mm diameter for ^{1}H imaging. The orthogonal arrangement minimized coupling between the ^{23}Na and the ^{1}H coil. The height of both coils was 11 mm. They were formed of 1-mm silver-plated copper wire (diameter 1 mm).

The ^{1}H coil facilitates shimming and positioning and provides anatomic images to be correlated with the measured sodium distribution pattern. A capacitive coupling scheme combined with triaxial baluns ensures full electrical balance of both circuits. At the ^{23}Na resonance frequency the isolation between the two channels is −37 dB. For the ^{23}Na channel, the quality factor Q of the unloaded probe is 238 falling to 196 when loaded with a 5-mm tube containing a physiological buffer solution. In the case of ^{1}H, the Q values of the empty/loaded coil are 414 and 360, respectively. Although an ideal coil should exhibit a much higher decrease of the quality factor upon insertion of the load, this situation is typical in NMR microscopy (*19*). Dealing with very small samples at high frequencies and with small coil sizes, electric losses in the coil and in the matching network are the dominating loss factors (*19*). The 90° pulse duration for the ^{23}Na coil was 7.0 μs at 300 W transmitter power corresponding to a $\vec{B}_1$ field strength of 2.96 mT.

After the shimming procedure using the ^{1}H signal, the linewidth in the global ^{23}Na spectrum was between 25 and 35 Hz. For ^{23}Na imaging, we chose a gradient echo sequence with a

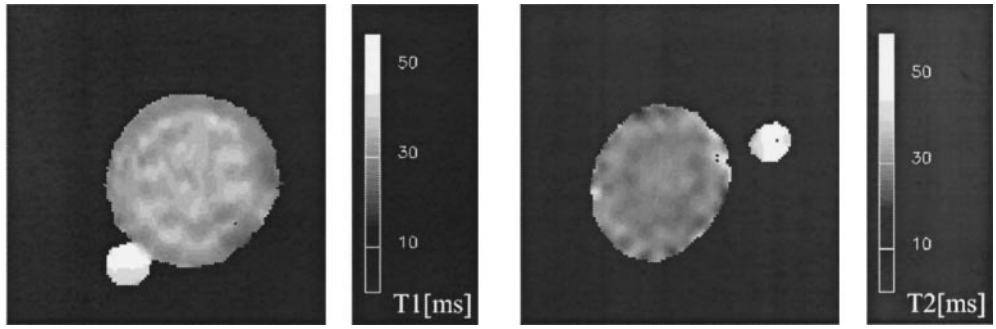

FIG. 2. Relaxation times of ^{23}Na in the cross section of the hypocotyl (FOV: 10 × 10 mm, matrix: 32 × 32, zero filled to 128 × 128, slice thickness: 10 mm). The T_1 map (left) was calculated out of eight T_1 weighted images acquired by an inversion recovery sequence (recovery time: 3.7–59.7 ms, TR: 200 ms). For the T_2 map eight spin-echo images were used (TE: 3.7–45.7 ms, TR: 200 ms).

flip angle of 90° and a repetition time (TR) of 50 ms. The sweep width was 10 kHz. Asymmetric echo sampling was used for a shorter echo time. With the center of the echo appearing after the first quarter of the acquisition window, echo time (TE) was 3.2 ms. A 5-mm transverse slice of the basal hypocotyl was selected with a 200-μs gaussian shaped pulse. We used CYCLOPS phase cycle and repeated each phase encoding step 1600 or 6400 times. A 64 × 64 (128 × 128) complex data matrix covered a FOV of 10 × 10 mm resulting in an isotropic nominal in-plane resolution of 156 μm (78 μm). Depending on the number of averages, the total experimental time was 85 min and 8.5 h.

Relaxation times of ^{23}Na were measured in the cross section of the hypocotyl of a seedling placed on 200 mM NaCl solution 36 h before the experiment was started. A 32 × 32 data matrix covered a FOV of 10 × 10 mm. Slice thickness was 10 mm. The T_1 map was calculated from eight T_1 weighted images produced by an inversion recovery sequence (recovery time: 3.7–59.7 ms, TR: 200 ms). For the T_2 measurement, a spin-echo sequence was used to acquire eight T_2 weighted images (TE: 3.7–45.7 ms, TR: 200 ms). Each phase encoding step was repeated 800 times resulting in a total experimental time of 12 h.

RESULTS

Anatomy

Figure 1 shows the hypocotyl anatomy of a 6-day-old castor bean seedling and compares a ^{1}H NMR microscopic image with a light microscopy of the same plant. The ^{1}H NMR image was obtained using a spin-echo sequence. It shows a 1-mm-thick slice of the hypocotyl. With a nominal in-plane resolution of 16 × 16 μm, the eight vascular bundles can be discerned in great detail. The cellular structures of the parenchymatic tissue are clearly visible.

Relaxation Times of ^{23}Na in the Plant

With a slice thickness of 10 mm and an in-plane resolution of 312 × 312 μm in the calculated T_1 and T_2 maps, the different tissue types showed no notable variation in relaxation times (Fig. 2). T_1 and T_2 of ^{23}Na in the cross section of the hypocotyl were found to be 33.1 ± 3.0 and 29.5 ± 2.9 ms (mean value and standard deviation of the entire stem). In comparison with the surrounding tissue, a slightly higher T_1 relaxation time constant as well as a lower T_2 value could only be observed in the area of the vascular ring.

^{23}Na NMR Microscopy

^{23}Na and ^{1}H images were acquired from about 20 seedlings *in vivo*. The plants had been exposed to NaCl concentrations between 25 and 300 mM for periods of time ranging from hours to days. Generally, we started 48 h before NMR investigation with a more moderate concentration and increased it the following day. Figure 3 monitors the marked differences in four plants, stressed to a variable extent with salt as seen in ^{23}Na NMR microscopy. In each case, the corresponding ^{1}H image is added below as anatomical reference. In all images the FOV was 10 × 10 mm. A projection of a 5-mm slice in case of ^{23}Na and of 1 mm in case of the ^{1}H is shown. In the ^{23}Na images, a nominal in-plane resolution of 156 × 156 μm has been reached within a total acquisition time of 85 min. With two averages the ^{1}H NMR experiment took 8.5 min. Comparing the mean value of signal intensity of the capillary (25 mM) with that of a region of the background, the signal-to-noise ratio in the ^{23}Na images was between 10 and 13.

Seedling (a) was placed on 300 mM NaCl solution 16 h before measurement. Under such strong saline conditions the plant survives only for a few hours. The eight light spots can be identified as xylem vessels, where the nutrient solution is transported upward. Less intensity occurs in the parenchymatic tissue distant from the vascular bundles. The center of the cortex parenchyma as well as the outer pith parenchyma ap-

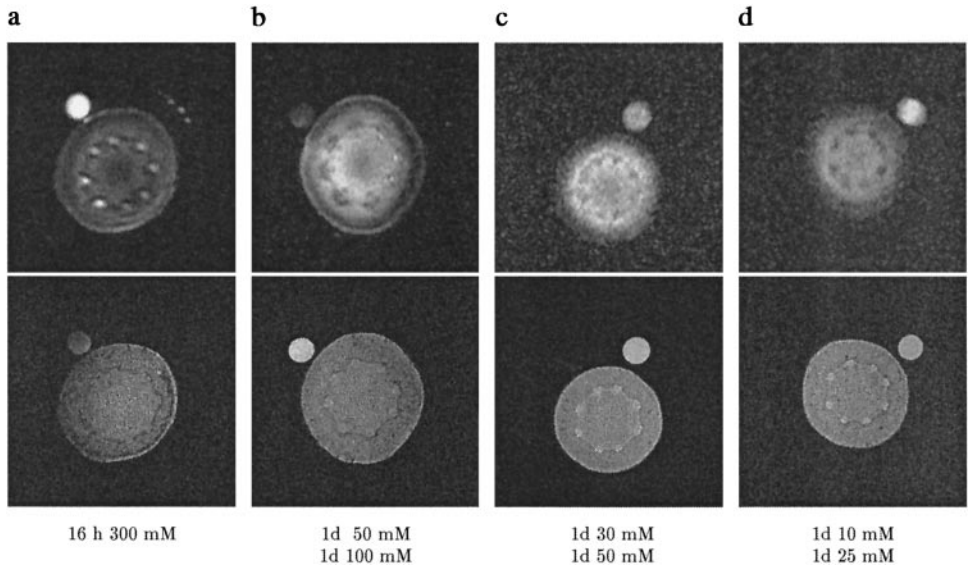

FIG. 3. ^{23}Na (top) and ^{1}H NMR microimages (bottom) of the hypocotyl base after exposure to different NaCl concentrations. FOV was 10 × 10 mm. ^{23}Na images were detected with a gradient echo sequence (TE: 3.2 ms, TR: 50 ms, flip angle 90°). From the 5-mm slice 64 × 64 data points were acquired, resulting in a nominal in-plane resolution of 156 × 156 μm. With 1600 averages the total experimental time was 85 min. The corresponding ^{1}H spin-echo images show a 1-mm slice detected with a 256 × 256 data matrix. All datasets were zero filled to 512 × 512.

pears quite dark while the epidermis is bright. NaCl concentration in the reference capillary was 100 mM in this case; in all other cases shown in Fig. 3 it was 25 mM.

When we incubated a seedling with a more moderate NaCl concentration for a longer period of time, a completely different compartmentalization of sodium occurred in the stem. Seedling (b) was grown on 30 mM for 1 day and on 100 mM for the following day. Again, signal strength is higher in the epidermis and in the parenchyma near the vascular bundles. In contrast to (a), the vascular bundles show poor intensity compared to the surrounding tissue. Remarkable are the half-moon-like structures near the phloem region. Plants (c) and (d) were exposed to 30/50 mM and 10/25 mM, respectively. At this concentration range, the seedlings grow without any salt effects. Both plants exhibited a similar sodium distribution pattern. While the xylem appears as a triangle of poor intensity, more signal comes from the phloem region. In contrast to the seedlings treated with a higher NaCl level, these plants exhibit a bright epidermis in the ^{23}Na images.

To check for the resolution limits of ^{23}Na NMR microscopy, we repeated the latter two experiments as "overnight measurements." Within 8.5 h, an in-plane resolution of 78 × 78 μm was achieved, as shown in Fig. 4. The signal-to-noise ratio was between 5 and 7. The results confirm the differences in the response of phloem and xylem as already seen in the lower resolved images.

The plant shown in Fig. 5 was grown on a vanishing external salt concentration in order to get a general idea of the threshold for detection of sodium by ^{23}Na NMR microscopy. Directly after germination, the seedling was transplanted from sodium-free medium to a nutrient solution containing 5 mM NaCl. With 9600 averages the acquisition of the image took 8.5 h. The region of the vascular bundles appears brighter than the surrounding parenchymatic tissue. By comparing the Na image

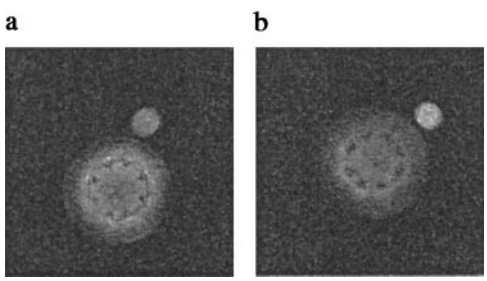

FIG. 4. ^{23}Na images with a nominal resolution of 78 × 78 μm and a slice thickness of 5 mm. Measurements were repeated with the same plants shown in Figs. 2c and 2d. Total acquisition time was 8.5 h (4800 averages).

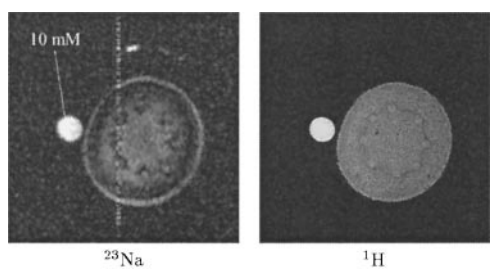

FIG. 5. ^{23}Na NMR microscopy under quasi-nonsaline conditions. (In-plane resolution: 156 × 156 μm, slice thickness: 5 mm, experimental time: 8.5 h). The vertical bright line is an image artifact due to HF contamination.

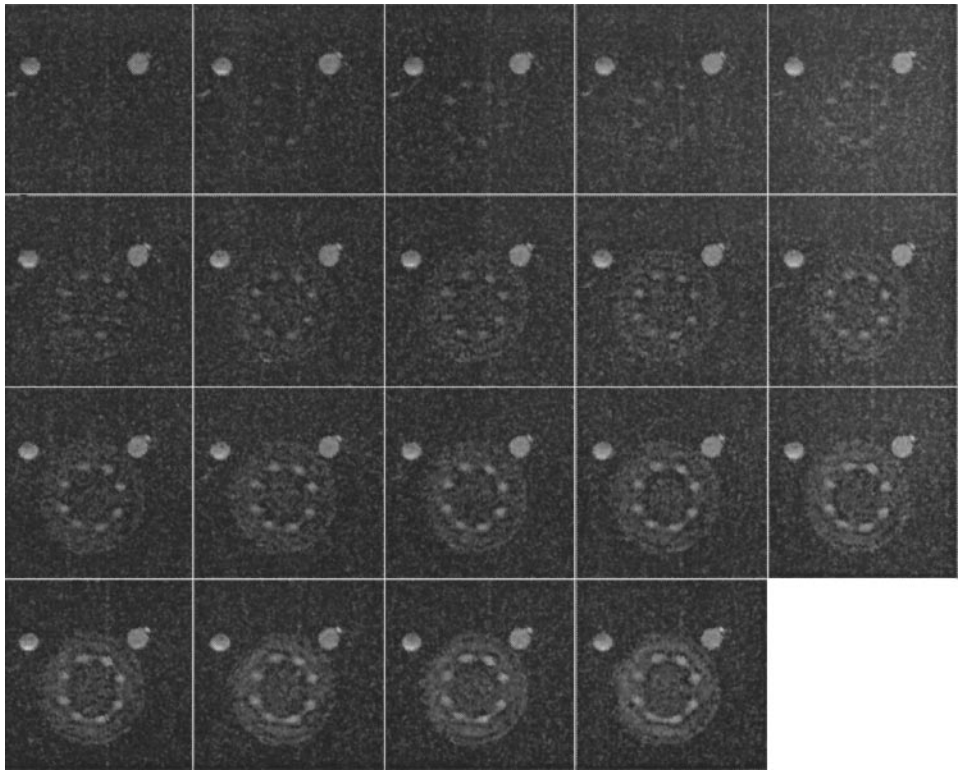

FIG. 6. Dynamical study of the time course of sodium uptake. ^{23}Na images were taken every 2 h after the addition of NaCl to the nutrient solution resulting in an external NaCl concentration of 200 mM.

with the corresponding anatomical image shown on the right, the triangular structures of low intensity can be associated with xylem vessels. The relatively high signal intensity of the epidermis is noteworthy. NaCl concentration in the capillary was 10 mM.

Time-Resolved Studies

The aim of these experiments was to follow the time course of sodium uptake. By alternately acquiring ^{23}Na and ^{1}H images, we observed dynamic changes in the physiological response of plants after salt treatment. Experimental parameters were the same as described above. One single ^{23}Na image was collected over 85 min. The following ^{1}H image took 8.5 min. The 19 subsequently acquired Na images of Fig. 6 display the progress of sodium uptake of the plant in real time. The first experiment was performed 1 h after the beginning of incubation with 200 mM NaCl. From image to image the interval was 2 h, covering a temporal range of 40 h. The sodium content of the reference capillaries was 50 mM (right) and 25 mM (left), respectively.

Already in the first images, signal intensity is increased in the vascular bundles. In the following, more and more signal also came from the parenchyma. In Fig. 7, the last image of the series is shown. The diagrams document the different tissue-specific reactions in the hypocotyl to salt stress.

Within the standard deviation, the signal strength of the reference capillary (25 mM) remained constant. In the vascular bundles, intensity increased fairly linearly. After 36 h, it reached the value of the reference. Signal strength of the pith parenchyma also went up, but remained by a factor of 6 below those of the vascular bundles. In the cortex parenchyma, most of the signal came from an annular ring between the region of the vascular bundles and the epidermis. In the outer tissue the kinetics of the sodium uptake was similar to that of the pith parenchyma.

DISCUSSION

For the first time, ^{23}Na NMR microscopy allows us to investigate the accumulation of sodium in specific tissue types as a function of salt stress of variable extent. With an experimental time of 85 min, we reached a spatial resolution in the ^{23}Na images of 156×156 μm, which is sufficient to differentiate the organs in the cross section of the hypocotyl. Because of the cylindrical geometry of the hypocotyl, a slice thickness of 5 mm can be accepted in the ^{23}Na images, even though a high resolution is used in-plane. A relatively thick slice and a high in-plane resolution is often beneficial for in NMR of plant stems in the cases of a poor signal-to-noise ratio (*14*) or a long acquisition time (*20*). Subsequently acquired ^{1}H images support the anatomical correlation of the ^{23}Na signal.

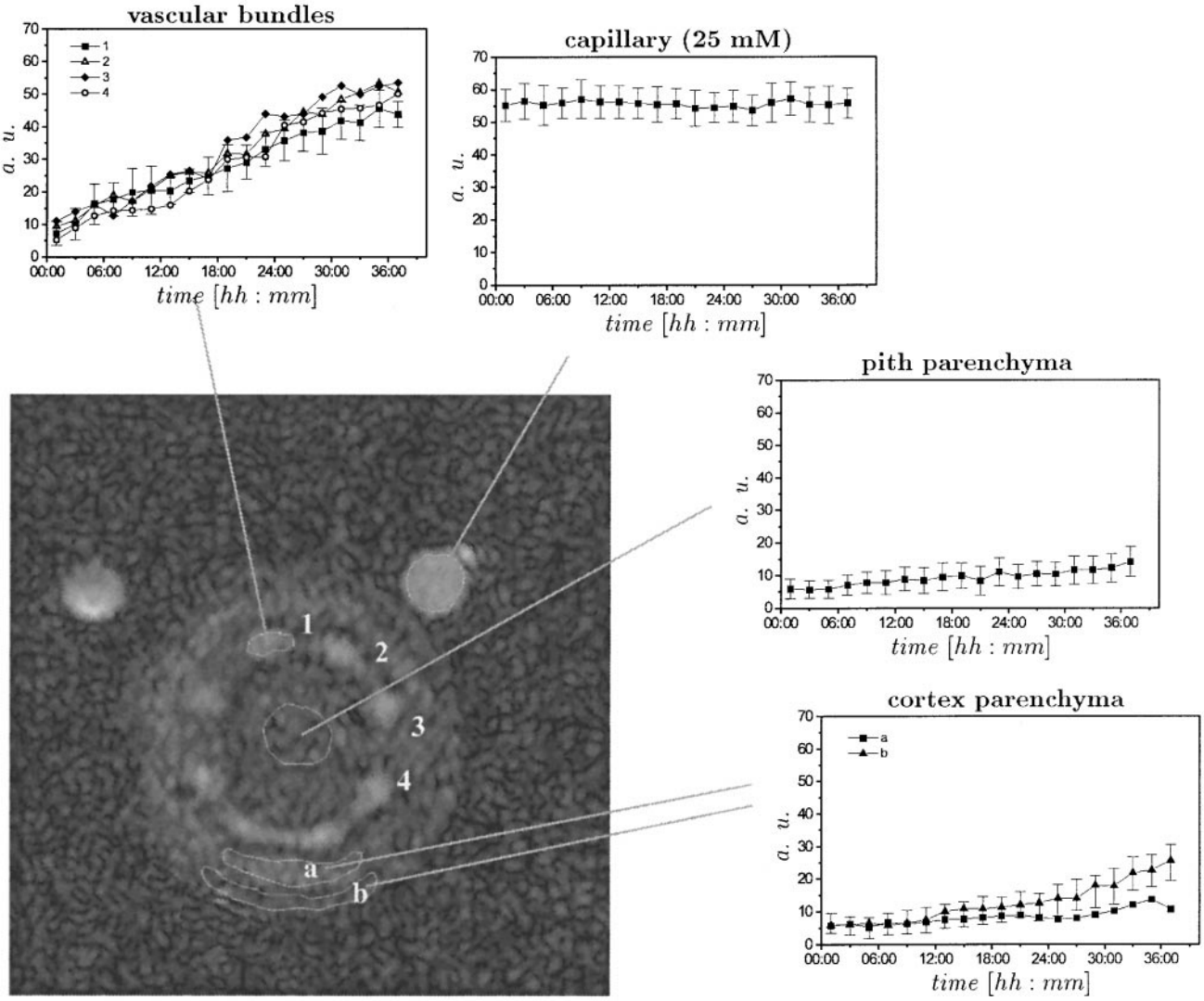

FIG. 7. Last image of the series in Fig. 5 monitoring the sodium distribution in the hypocotyl after 39 h of NaCl incubation. Shown are mean values and standard deviations of signal intensities of the marked segments. All graphics are scaled equally.

In the images shown in Fig. 4, we achieved an in-plane resolution of 78 × 78 μm, although with 50 and 25 mM, the external salt concentration was moderate. This is the highest resolution reached so far in a ^{23}Na NMR image. These experiments document the high potential of ^{23}Na NMR imaging for tissue-specific observation of a plant under salt stress. However, with an experimental time of 8.5 h, the status of physiological equilibrium might not be guaranteed during measurement. Since the 156 × 156 μm images already provide the spatial information necessary for anatomical details, those investigations with an experimental time of 85 min are preferable for standard measurements.

The sensitivity of ^{23}Na NMR imaging appeared to be high enough to localize sodium in the castor bean seedling even under quasi-nonsaline conditions (5 mM external NaCl concentration). Obviously, the physiological response of a plant to salt strongly depends on the extent of stress, concentration, and duration of incubation. When the seedling is exposed to a very high NaCl concentration, the sodium enters mainly the xylem vessels (Fig. 3a). Under more moderate conditions, the sodium seems to be excluded from the phloem region (Fig. 3b). Whenever the seedlings were grown on a salt concentration which they could survive long term without any visible physiological damage, the region of the xylem exhibited only low signal strength compared to the surrounding tissue. Possibly, the plant is able to transport the sodium out of the vessels of the xylem and store it in the surrounding tissue. In this way, the plant could inhibit the sodium from reaching the leaves. Another possible path of Na^+ might be retranslocation from the leaves to the stem via the phloem, which was already shown in adult Ricinus plants (*21*).

The temporal course of the sodium intensity in the hypocotyl

of a seedling shocked with a high salt concentration (200 mM) can be observed spatially resolved. Sodium uptake and further spread in tissue develops over a time scale much longer than the duration of a single experiment (85 + 8.5 min). The present results prove that the dynamics of sodium uptake is easily accessible by ^{23}Na NMR imaging. Further studies could focus on the impact of the external salt concentration on the kinetics. An investigation on the longer term—over the range of several days—could be performed in order to check whether an equilibrium distribution occurs. A systematic study of the kinetics of sodium accumulation in xylem, phloem, and parenchymatic tissue under various saline conditions could be very instructive for a fundamental understanding of salt stress on the macroscopic level. Essential for this purpose is the use of a climate chamber probehead wherein the environmental conditions can be controlled. When the studies described in this paper were performed, the design of the climate chamber was still in progress. Since then, a newer climate chamber has been developed which allows the control of humidity and illumination as well as the measurement of temperature, aspiration, and respiration of the seedlings.

CONCLUSION

The results of the present studies prove the capacity of ^{23}Na NMR microimaging for functional dynamic analysis of salt stress in plants. For the first time, the sodium distribution in an unperturbed living plant can be visualized, whereby the spatial resolution achieved (156 μm in-plane) allows one to distinguish the behavior of different tissue types. Depending on the level of external NaCl concentration and the duration of incubation, the tissue-specific response can be analyzed.

An experimental time of 85 min is short compared to the time scale of the physiological response of the plant to salt stress. Thus, ^{23}Na NMR provides temporal information sufficient for kinetic studies without a loss in spatial resolution. The sensitivity of this technique is sufficient to detect the sodium distribution pattern even at very low external salt concentrations (5 mM). This concentration threshold lies far below the critical NaCl concentration of 100 mM.

The values for T_1 and T_2 of ^{23}Na in the plant were found not to vary notably for the different tissue types. Therefore, on first sight, relaxation time weighting should be of no meaning in ^{23}Na images and signal intensity in the ^{23}Na images should mainly reflect the sodium content. However, T_2 was measured using a minimum TE of 3.7 ms. For that reason, the fast relaxing T_2 component (which likely has a T_2 shorter than 3 ms) did not contribute to the signal in either the relaxation time maps or the ^{23}Na images. A possible variation of the relative contribution of fast and slow relaxing components in different tissue compartments would produce T_2 weighting due to partial NMR invisibility of the ^{23}Na.

Additionally, in order to obtain a sufficient signal-to-noise ratio, the relaxation time measurements were made using 10-mm-thick slices collected over 12 h, as opposed to 5-mm-thick slices collected over 85 min in all ^{23}Na imaging work. The different measurement times also mean different sodium exposure times, which also might have an effect on the relaxation properties of ^{23}Na. This might complicate the quantitative analysis of ^{23}Na concentration.

With this in mind, a declaration of quantitative values of the sodium concentration in the organs of the plant using the capillary for calibration is not straightforward. One must not only correct for the $\vec{B}_1$ inhomogenity of the coil, but also consider the visibility problem of ^{23}Na in biological tissue. The visibility factors of ^{23}Na in the plant must be determined carefully since they may be markedly different for each tissue type. Therefore, the knowledge of the value of the fast T_2 and its relative contribution is essential for absolute quantification of the ^{23}Na NMR signal intensity. Nevertheless, the signal-to-noise ratio of about 10 in the ^{23}Na images implicates that absolute quantification of the sodium content in tissue by ^{23}Na NMR imaging might be a promising approach in further studies.

In conclusion, ^{23}Na NMR microimaging may fill the gap of *noninvasive* characterization of salt sensitive and salt-tolerant crops under different environmental conditions. This technique could become the method of choice for characterizing salt-sensitive as well as salt-tolerant crops and understanding their different physiological reactions.

ACKNOWLEDGMENTS

We thank B. Kalusche (Experimentelle Physik V, Universität Würzburg) for his advice for the probehead design and for fruitful discussions accompanying all studies. This work was supported by a grant from the Deutsche Forschungsgemeinschaft to A.H. and E.K.

REFERENCES

1. T. J. Flowers and A. Läuchli, Sodium versus potassium: Substitution and compartmentation, *in* "Encyclopedia of Plant Physiologie" (U. Lüttge and M. G. Pitman, Eds), New Series, Vol. 15B, pp. 651–681, Springer-Verlag, Berlin (1983).
2. L. O. Sillerud and J. W. Heyser, Use of ^{23}Na-NMR to follow sodium uptake and efflux in NaCl-adapted and nonadapted millet (*Panicum Miliaceum*) suspensions, *Plant Physiol.* **75,** 269–272 (1984).
3. L. Packer, S. Spath, J. B. Martin, C. Roby, and R. Bligny, ^{23}Na and ^{31}P NMR studies of the effects of salt stress on the freshwater cyanobacterium *Synechococcus* 6311, *Arch. Biochem. Biophys.* **256**(1), 354–361 (1987).
4. M. Bental, H. Degani, and M. Avron, ^{23}Na-NMR studies of the intracellular sodium ion concentration in the halotolerant alga *Dunaliella Salina, Plant Physiol.* **87**(4), 813–817 (1988).
5. W. V. Gerasimowicz, S. I. Tu, and P. E. Pfeffer, Energy facilitated Na^+ uptake in excised corn roots via ^{31}P and ^{23}Na NMR, *Plant Physiol.* **81**(3), 925–928 (1986).
6. T.-W. M. Fan, R. M. Higashi, J. Norlyn, and E. Epstein, *In vivo* ^{23}Na and ^{31}P NMR measurement of a tonoplast Na^+/H^+ exchange pro-

cess and its characteristics in two barley cultivars, *Proc. Natl. Acad. Sci. USA* **86**(24), 9856–9860 (1989).

7. C. M. Spickett, N. Smirnoff, and R. G. Ratcliffe, An *in vivo* nuclear magnetic resonance investigation of ion transport in maize (Zea mays) and Spartina anglica roots during exposure to high salt concentrations, *Plant Physiol.* **102,** 629–638 (1993).
8. H. Kano, N. Ishida, H. Takagishi, K. Shirata, and M. Koizumi, Tracing effects of Na^+ on morphology, phosphate metabolism and accumulated compounds of a sugar beet root by NMR, *Jpn. J. Crop Sci.* **62**(1), 95–104 (1993).
9. R. K. Gupta and P. Gupta, Direct observation of resolved resonances from intra cellular and extracellular sodium-23 ions in nmr studies of intact cells and tissues using Dysprosium(III)tripolyphosphate as para magnetic shift reagent, *J. Magn. Reson.* **47,** 344–350 (1982).
10. R. G. Ratcliffe, *In vivo* NMR studies of higher plants and algae, *in* "Advances in Botanical Research," Vol. 20 (J. A. Callow, Ed), pp. 41–108, Academic Press, London (1994).
11. M. Koizumi, N. Ishida, H. Takagishi, K. Shirata, and H. Kano, Observation of water and Na^+ in tissues of the *Bruguiera Gymnorrhiza* by ^{1}H- and ^{23}Na-NMR imaging, *Bot. Mag. Tokyo* **105**(1077), 1–11 (1992).
12. C. S. Springer, Jr., Measurement of metal cation compartmentalization in tissue by high-resolution metal cation NMR, *Annu. Rev. Biophys. Biophys. Chem.* **16,** 375–399 (1987).
13. J. Verscht, B. Kalusche, J. Köhler, W. Köckenberger, A. Metzler, A. Haase, and E. Komor, The kinetics of sucrose concentration in the phloem of individual vascular bundles of the *Ricinus communis* seedling measured by nuclear resonance microimaging, *Planta* **205,** 132–139 (1998).
14. M. Heidenreich, W. Köckenberger, R. Kimmich, N. Chandrakumar, and R. Bowtell, Investigation of carbohydrate metabolism and transport in castor bean seedlings by cyclic *J* cross polarization imaging and spectroscopy, *J. Magn. Reson.* **132,** 109–124 (1998).
15. W. Köckenberger, J. M. Pope, Y. Xia, K. R. Jeffrey, E. Komor, and P. T. Callaghan, A non-invasive measurement of phloem and xylem water flow in castor bean seedlings by nuclear magnetic resonance microimaging, *Planta* **201**(1), 53–63 (1997).
16. A. Ziegler, A. Metzler, W. Köckenberger, M. Izquierdo, E. Komor, A. Haase, M. Decorps, and K. M. Von, Correlation-peak imaging, *J. Magn. Reson. B* **112**(2), 141–150 (1996).
17. A. Metzler, W. Köckenberger, K. M. Von, E. Komor, and A. Haase, Quantitative measurement of sucrose distribution in *Ricinus communis* seedlings by NMR chemical-shift microscopy, *J. Magn. Reson. B* **105,** 249–252 (1994).
18. E. Kuchenbrod, M. Landeck, F. Thürmer, A. Haase, and U. Zimmermann, Measurement of water flow in the xylem vessels of intact maize plants using flow-sensitive NMR imaging, *Bot. Acta* **108,** 184–186 (1996).
19. D. I. Hoult and R. E. Richards, The signal-to-noise ratio of the nuclear magnetic resonance experiment, *J. Magn. Reson.* **24,** 71–85 (1976).
20. M. Meininger, P. M. Jakob, M. v.Kienlin, D. Doppler, G. Bringmann, and A. Haase, Radial spectroscopic imaging, *J. Magn. Reson.* **125,** 325–331 (1997).
21. W. B. Jeschke and J. S. Pate, Cation and chloride positioning through xylem and phloem within the whole plant of *Ricinus communis* L. under conditions of salt stress, *Exp. Bot.* **42,** 1105–1116 (1991).